Ultra-high-resolution paleoenvironmental records via direct laser-based analysis of lipid biomarkers in sediment core samples

Lars Wörmer[a,1], Marcus Elvert[a], Jens Fuchser[b], Julius Sebastian Lipp[a], Pier Luigi Buttigieg[a,c], Matthias Zabel[d], and Kai-Uwe Hinrichs[a,1]

[a]Organic Geochemistry Group, MARUM Center for Marine Environmental Sciences and Department of Geosciences, University of Bremen, 28359 Bremen, Germany; [b]Fourier Transform Mass Spectrometry Applications-Development, Bruker Daltonik GmbH, 28359 Bremen, Germany; [c]Helmholtz-Gemeinschaft Max-Planck-Gesellschaft Research Group on Deep-Sea Ecology and Technology, Alfred–Wegener-Institut Helmholtz–Zentrum für Polar- und Meeresforschung, 27570 Bremerhaven, Germany; and [d]Inorganic Geochemistry Group, MARUM Center for Marine Environmental Sciences and Department of Geosciences, University of Bremen, 28359 Bremen, Germany.

Edited by Katherine H. Freeman, Pennsylvania State University, University Park, PA, and approved September 23, 2014 (received for review March 24, 2014)

Marine microorganisms adapt to their habitat by structural modification of their membrane lipids. This concept is the basis of numerous molecular proxies used for paleoenvironmental reconstruction. Archaeal tetraether lipids from ubiquitous marine planktonic archaea are particularly abundant, well preserved in the sedimentary record and used in several molecular proxies. We here introduce the direct, extraction-free analysis of these compounds in intact sediment core sections using laser desorption ionization (LDI) coupled to Fourier transform ion cyclotron resonance mass spectrometry (FTICR-MS). LDI FTICR-MS can detect the target lipids in single submillimeter-sized spots on sediment sections, equivalent to a sample mass in the nanogram range, and could thus pave the way for biomarker-based reconstruction of past environments and ecosystems at subannual to decadal resolution. We demonstrate that ratios of selected archaeal tetraethers acquired by LDI FTICR-MS are highly correlated with values obtained by conventional liquid chromatography/MS protocols. The ratio of the major archaeal lipids, caldarchaeol and crenarchaeol, analyzed in a 6.2-cm intact section of Mediterranean sapropel S1 at 250-μm resolution (∼4-y temporal resolution), provides an unprecedented view of the fine-scale patchiness of sedimentary biomarker distributions and the processes involved in proxy signal formation. Temporal variations of this lipid ratio indicate a strong influence of the ∼200-y de Vries solar cycle on reconstructed sea surface temperatures with possible amplitudes of several degrees, and suggest signal amplification by a complex interplay of ecological and environmental factors. Laser-based biomarker analysis of geological samples has the potential to revolutionize molecular stratigraphic studies of paleoenvironments.

molecular stratigraphy | solar cycle | laser desorption ionization | FTICR-MS | archaeal tetraether lipids

Microbial lipids in aquatic sediments reflect phylogeny, environmental conditions, and biogeochemistry of the water column in which they were produced. After sedimentation and because of the persistence of lipid structures in the sedimentary record, the information archived in these lipids remains available on geological time scales. Retrieval of this information from sediments and rocks has increasingly contributed to our understanding of past environments, microbial communities, and biogeochemical processes (e.g., refs. 1–5). Merged with the concept of molecular stratigraphy (2, 6), i.e., the analysis of selected biomarkers in solvent extracts of sediment samples in a stratigraphic framework, unique information can be gleaned regarding the temporal changes of past ecological and environmental conditions in aquatic systems. Because of analytical requirements, the temporal resolution is typically limited by centimeter-scale-sized samples, which, dependent on the depositional setting, tend to integrate time periods of decades to millennia, even in high-sedimentation settings such as the Santa Barbara Basin (e.g., refs. 4, 7, 8). In consequence, our knowledge of the temporal changes of the environmental and ecological history recorded by lipid biomarkers is rather coarse and based on long-term averages of their distributions in the sedimentary record.

In this study we seek to extend this approach to ultra-high-resolution molecular stratigraphy. We focused on archaeal glycerol dialkyl glycerol tetraethers (GDGTs), which are produced by planktonic archaeal communities and are ubiquitous and persistent components in marine sediments (e.g., refs. 9, 10) with widely recognized potential for paleoenvironmental studies. The number of cycloalkyl rings in GDGTs (Fig. S1) appears highly sensitive to ecological and environmental factors such as phylogeny (ref. 5 and references therein), temperature (ref. 11 and references therein), or pH (12, 13). This sensitivity of GDGT composition to environmental and ecological factors has driven the development of multiple molecular proxies. Adaptation to temperature has been demonstrated in thermophilic cultures of archaea (e.g., ref. 14) and serves as concept for the reconstruction of paleo sea surface temperatures (SST) in sediments using the TEX_{86} (tetraether index of 86 carbon atoms) (3), which is based on fossil lipids of planktonic archaea. This proxy has been used to characterize oscillations of SST in different geological episodes (e.g.,

Significance

Lipid biomarkers in geological samples are important informants regarding past environments and ecosystems. Conventional biomarker analysis is labor intensive and requires relatively large sediment or rock samples; temporal resolution is consequently low. Here, we present an approach that has the potential to revolutionize paleoenvironmental biomarker research; it avoids wet-chemical sample preparation and enables analysis of biomarkers directly on sediment cores at submillimeter spatial resolution. Our initial application to a sediment core deposited during the Holocene climate optimum in the Mediterranean Sea reveals a new view of how small-scale variations in lipid distribution are integrated into commonly reported signals obtained by conventional analysis and demonstrates a strong influence of the ∼200-y de Vries solar cycle on sea-surface temperatures and planktonic archaeal ecology.

Author contributions: L.W., M.E., and K.-U.H. designed research; L.W., M.E., J.F., and M.Z. performed research; L.W., J.S.L., P.L.B., M.Z., and K.-U.H. analyzed data; J.F. contributed new reagents/analytic tools; and L.W. and K.-U.H. wrote the paper.

The authors declare no conflict of interest.

This article is a PNAS Direct Submission.

Data deposition: Data has been deposited in the Pangaea database, www.pangaea.de (doi: 10.1594/PANGAEA.836387).

[1]To whom correspondence may be addressed. Email: khinrichs@uni-bremen.de or lwoermer@marum.de.

This article contains supporting information online at www.pnas.org/lookup/suppl/doi:10.1073/pnas.1405237111/-/DCSupplemental.

refs. 8, 15, 16). Complications could arise from additional GDGT sources, e.g., allochthonous inputs of GDGT-bearing soils, lateral transport, in situ production, and/or recycling by sedimentary archaea (cf. refs. 5, 17). Relative GDGT distributions required for proxy calculations are obtained by HPLC atmospheric pressure chemical ionization mass spectrometry (HPLC/APCI-MS) of solvent extracts from gram-sized sediment samples (18, 19).

To enhance temporal resolution of GDGT-based proxies, we explored the utility of laser desorption ionization coupled to Fourier transform ion cyclotron resonance mass spectrometry (LDI FTICR-MS). In LDI, the impact of a pulsed laser beam on the sample leads to desorption, vaporization and ionization of the analytes, forming a cloud of charged molecules. An additional matrix is frequently applied to facilitate the generation of ions (matrix assisted laser desorption ionization [MALDI]). A complete understanding of underlying ionization mechanisms has not been achieved yet (20). LDI or MALDI are best known in the field of proteins or peptides and have also been successfully used in lipid research (21). The fact that LDI analysis can generate ions directly from the sample placed on a sample holder without time-consuming wet-chemical pretreatment while producing mass spectra from submillimeter-sized spots (as small as 10 μm) makes this technique particularly attractive for molecular stratigraphy. LDI may allow direct analysis of nanogram-sized samples on the surface of cut, intact sediment cores at ultra-high spatial resolution, equivalent to temporal resolution on the order of months to decades.

We aimed to develop a technique that takes advantage of both the exquisite sensitivity and unequivocal molecular information of ultra-high-resolution mass spectrometry by FTICR-MS and the high spatial resolution of LDI within an intact and unaltered sedimentological context. The key steps of validation and implementation included (Fig. S2) (*i*) the detection of archaeal GDGTs, (*ii*) verification of results obtained by LDI FTICR-MS by parallel analysis using established HPLC/APCI-MS methods, and (*iii*) the examination of the first continuous high-resolution GDGT profile from a sediment core section of the eastern Mediterranean sapropel S1, which was deposited under anoxic conditions during the Holocene climatic optimum (HCO; refs. 22, 23). The data thus may provide an unprecedented view of the dynamic variations of both SST and ecological and environmental factors during sapropel formation.

Results and Discussion

Successful Detection of GDGTs by LDI FTICR-MS. Analyses of a ground sapropel sample with high abundance of GDGTs confirmed the capacity of LDI FTICR-MS to efficiently ionize and unequivocally identify GDGTs, which were observed exclusively in the form of Na^+ adducts. The high resolving power of FTICR-MS is crucial for accurate identification, as the *m/z* value of the second isotopic peak of any given GDGT with *n* cycloalkyl moieties will be very close to the *m/z* of a GDGT with *n-1* cycloalkyl moieties (Fig. S3). We furthermore demonstrated that the tested artificial matrices, as applied during MALDI, did only slightly enhance ionization (Fig. S4, see *Supporting Information* for more details). We therefore chose to perform our experiments without matrix to avoid negative effects with sample preparation, including diffusion of matrix into the sediment, which could result in lipid solubilization and thus loss of spatial resolution.

GDGT Distributions: HPLC/APCI-MS vs. LDI FTICR-MS. We compared the relative abundance of different GDGT species in 21 ground samples from the Mediterranean, Marmara, and Black seas obtained by conventional HPLC/APCI-MS and LDI FTICR-MS. We primarily focused on a readily accessible ratio of the two major core lipids, GDGT-0 (caldarchaeol) and GDGT-5 (crenarchaeol), in the form of a crenarchaeol–caldarchaeol tetraether index (CCaT; Eq. **1**). This ratio is known to be sensitive to SST variations (3) and possibly to changes in archaeal community composition due to the prominence of caldarchaeol in diverse cren-, thaum-, and euryarchaeota vs. the restricted occurrence of crenarchaeol in marine thaumarchaeota (24, 25). We obtained a strong linear correlation ($r^2 = 0.97$; $P < 0.0001$), with a slope of 1.056, demonstrating the robustness of the LDI method (Fig. 1; Eq. **S1**). SST reconstruction via the extensively studied SST proxy TEX_{86} (Eq. **S2**), which integrates the abundance of minor GDGTs including the regioisomer GDGT-5′, is not possible by LDI FTICR-MS because *m/z* values of GDGT-5 and its less abundant regioisomer GDGT-5′ (see Fig. S1 for structures) are identical.

$$\mathrm{CCaT} = \left([5] + [5']\right) / \left([0] + [5] + [5']\right). \quad [1]$$

We also evaluated a ratio that includes the minor GDGTs for validation of the LDI-based approach. We chose the methane index (MI; Eq. **S3**; ref. 26), which is considered to be sensitive to the contribution of GDGTs derived from anaerobic methane-oxidizing archaea. Results from LDI analysis are strongly correlated with those obtained by HPLC/APCI-MS analysis of extracts ($r^2 = 0.78$, $P < 0.0001$), with the slope of the linear regression being 0.956 (Fig. S5*A*; Eq. **S4**). The offset between both methods, with LDI-based MI values being consistently higher than the LC-based counterparts, is possibly due to overestimation of GDGT-1 with the LDI approach due to codetection of unsaturated GDGT-0, which may be formed by dehydration of hydroxylated GDGT-0 (27).

SST Sensitivity of the CCaT. SST sensitivity of the CCaT was examined based on available global LC-based calibration datasets (28, 29). We obtained an SST calibration for the CCaT for the temperature range from 5 to 30 °C ($r^2 = 0.70$, $P < 0.0001$; Fig. S5*B*; Eq. **S5**). The strength of the correlation, compared with the TEX_{86} (3) and its derivatives (28), is somewhat weaker and suggests that additional factors such as planktonic archaeal ecology are also reflected in the CCaT. However, independent indirect support for an SST sensitivity of the LDI-based CCaT comes from further examination of the 21-sample set where the CCaT is strongly

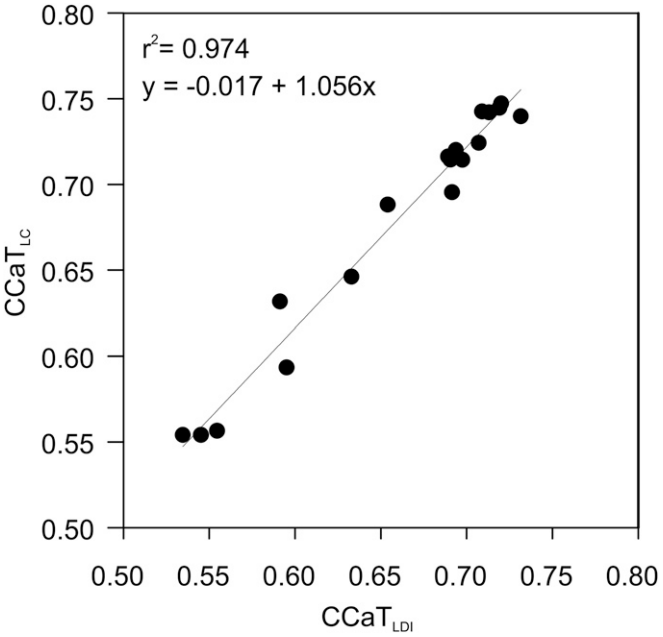

Fig. 1. Correlation between LDI FTICR-MS and HPLC/APCI-MS measurements of the CCaT; 21 sediment samples retrieved during *Meteor* cruise M84-1 (Table S1) were used to test linear correlation of LDI and HPLC/APCI-MS measurements.

correlated with the LC-based TEX_{86} ($r^2 = 0.95$, $P < 0.0001$; Fig. S5*C*; Eq. **S6**).

High-Resolution Analysis of an Intact Sediment Core Section. We acquired >4,000 individual mass spectra of GDGT distribution in 250-μm intervals of 175-μm sized laser spots (with 75 μm distance between spots) in a 6.2 × 0.6 cm intact sediment core section from the Mediterranean sapropel S1 (Fig. 2*A*). For the two major compounds required for the CCaT, GDGT-0 and GDGT-5, we obtained 3,047 valid spectra (signal-to-noise ratio, SNR > 5; cf. Fig. 2B and Dataset S1), corresponding to an average of about 15 valid spectra in each horizontal layer. The two minor compounds GDGT-1 and GDGT-2 were observed in adequate abundance (SNR > 5) in 38% of all spectra, and GDGT-3 in only 13% of the spectra.

To characterize the spatial patterns in our data across all scales, we explored potential suitability of principal coordinates of neighbor matrices (PCNM) analysis (30–32). When used as explanatory variables in a partial redundancy analysis, the complete set of PCNM variables constrained ~56% of the variation in the CCaT data, thus suggesting the presence of meaningful spatial patterns, both coarse and fine grained, in the dataset (see *Supporting Information* and Fig. S6 for more details).

The variations of the CCaT on a small spatial scale provide an unprecedented perspective on how normal-sized sediment samples integrate highly diverse signals into seemingly homogenous distributions (e.g., ref. 16). The CCaT data range (defined as average ±2 SD, equivalent to 95.4% of recorded data) obtained from the surface of the ~2-cm^3 sample, i.e., a volume not untypical for a single sample in molecular proxy studies, covers values from 0.53 to 0.87 and data follow a Gaussian distribution (Fig. S7*A*). This rivals the CCaT range observed in the global dataset (28) (Fig. S7*B*). We also evaluated the CCaT ranges in individual horizontal layers, defined by minima and maxima after elimination of data outside the mean ± 2σ range. Throughout the analyzed section, dispersion of CCaT values within these 0.25 × 5-mm horizontal layers is high (Fig. S7*C*), with average single horizons ranging from 0.58 to 0.82, corresponding to SST estimates of 19.8–36.2 °C (Fig. S7*B*). For comparison, modern monthly averaged SST in this area for the period 1955–2012 ranges from 16.8 °C in March to 27.2 °C in August (33). The southeastern Mediterranean region during the HCO was generally warmer and more humid than today (34), and reduced vertical mixing in the stratified water column during sapropel formation may have promoted higher summer peak SST. Despite large dispersion of individual measurements, the SST estimates derived from average and median values of 0.698 and 0.704, respectively (27.9 and 28.3 °C) closely match values obtained from sapropel S1 sediments in this region by conventional TEX_{86} analysis, which were interpreted to represent summer SST (~28 °C; ref. 16).

Although the average CCaT fits summer SST, the large range as well as the patchiness of the spatial distribution of values is consistent with accumulation of GDGT-bearing particles during all seasons. At the same time, the magnitude of the observed range argues against temperature being the only control of the CCaT distribution. We suggest that factors such as (*i*) contribution of different members of the planktonic archaeal community: euryarchaeota vs. thaumarchaeota (e.g., refs. 35, 36) and deep vs. shallow thaumarchaeota (37), and (*ii*) production and export of GDGT-bearing particle fluxes from different water column depths (38–40) have contributed to this wide range. It is interesting to note that similar effects are observed when reducing sample sizes in oxygen isotopic analysis of foraminiferal calcite; single-species $\delta^{18}O$ values scatter widely in narrow sediment intervals, with the large range presumably representing seasonal and interannual changes in temperature and hydrologic patterns, as well as vertical distribution of habitats in the water column (41, 42).

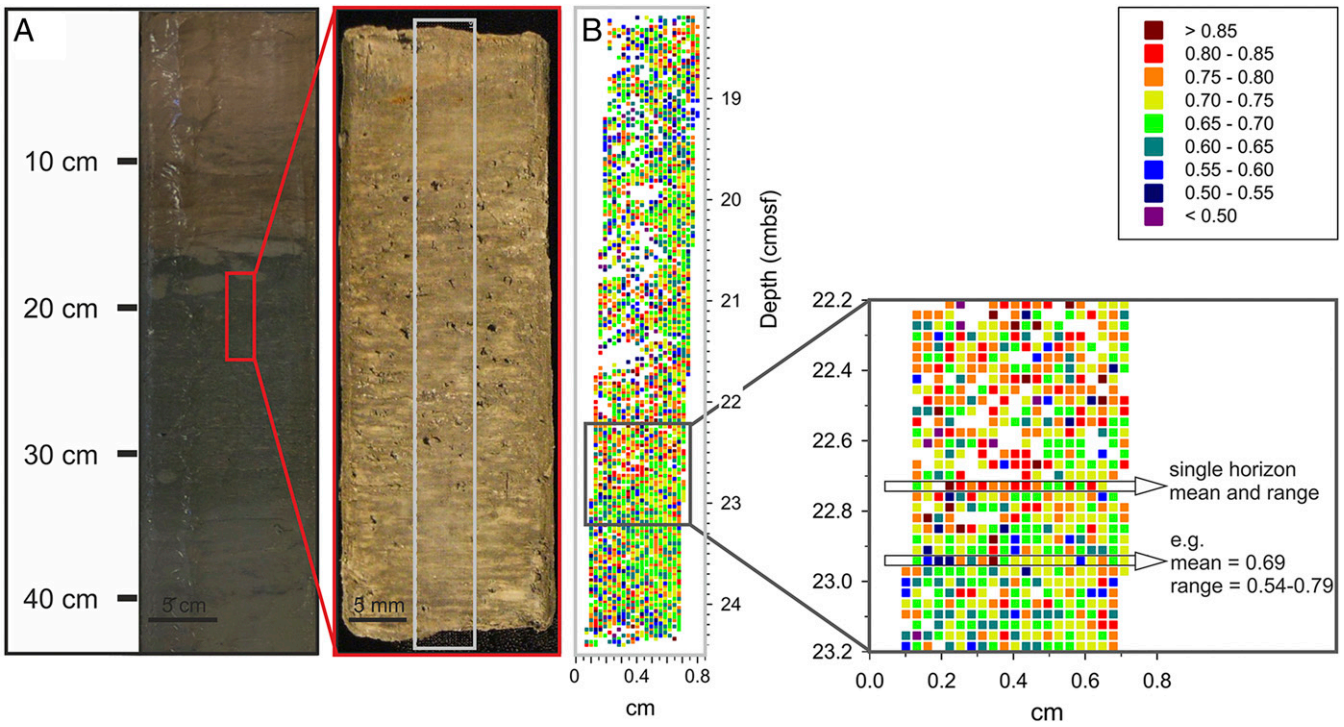

Fig. 2. (*A*) Photograph of sediment section of core GeoB 15103–1 (eastern Mediterranean Sea) used for high-resolution LDI FTICR-MS analysis. The section corresponds to the upper part of sapropel 1. (*B*) CCaT values for each analyzed spot, exemplary zoom-in, and average and range values for two selected horizontal layers. White fields in figure indicate spots in which GDGTs could not be detected in sufficient concentration, possibly due to inefficient ionization.

Temporal Variations of GDGT Distributions. The downcore profile of GDGT distribution was obtained by averaging individual measurements of each horizontal layer to a single reported data point (Fig. 2*B*). Even though sapropel S1 was deposited under relatively low sedimentation rates (see *Supporting Information* for sedimentation rate estimation), the lack of bioturbation caused by anoxia combined with our spatial resolution translates into a temporal resolution of ∼4 y. Horizontal averages of the CCaT range from 0.59 to 0.79, which correspond to SST estimates of 20.5–33.8 °C (Fig. 3*A*). Analytical uncertainty for these measurements was estimated by 122 data points of a ground sediment sample as 0.026 CCaT ratio units (2 σ) (*Supporting Information*). A similar SST range is obtained when converting the CCaT into TEX_{86} according to Eq. **S6** and applying the calibration proposed for SST estimations in warm (SST > 15 °C) regions or periods (ref. 28; Eq. **S7**). A smoothed seven-point running average curve, equivalent to ∼30-y SST averages of 24.1–30.7 °C, emphasizes the potential presence of a cyclic forcing of the GDGT distribution, which we will further examine in the next section. The estimated high SST are suggestive of significant warming during S1 deposition, which coincides with the HCO (34) and may also reflect increased seasonality during warm episodes (16, 43).

Although SST is an important factor influencing the GDGT distribution, the variations of the CCaT likely integrate additional forcing factors that amplify its cyclic signal amplitudes. These alternative factors include regular shifts in contributions of different archaeal ecotypes (35, 36) that may influence the relative amounts of GDGT-0 and -5 (5). When the annual SST range is large, a recurring shift in the seasonality of GDGT production and export could also result in strongly altered CCaT values. Dimly lit chemoclines are considered to be locations of intensified thaumarchaeal production (38, 44) and short-term, cyclic changes in water-column stratification, redox conditions, and nutrient and light regimes may result in varying GDGT fluxes from different depths.

The individual methanotrophy-sensitive MI_{LDI} values mostly range from 0.28 to 0.40 (Fig. S8). Liquid chromatography-based values above MI = 0.3 indicate significant contribution of GDGTs from methanotrophic archaea (26), for example, due to enhanced methane flux and associated intensification of anaerobic oxidation of methane in the sediment. Correcting for the slightly elevated values obtained through LDI (Eq. **S4**), the threshold indicating substantial methane influence would be placed at an MI_{LDI} of 0.39. High rates of sedimentary methanotrophy are an implausible explanation for the relatively high MI values at this location because sapropel S1 is placed well in the sulfate-reduction zone at seawater-like sulfate concentrations combined with a high sulfate penetration depth (45) and extremely low methane concentrations (46), all these factors being consistent with low fluxes of methane. Thus, the elevated MI values may reflect enhanced methane oxidation in the stratified, anoxic water column during sapropel formation, as has been described in the modern euxinic Black Sea (47).

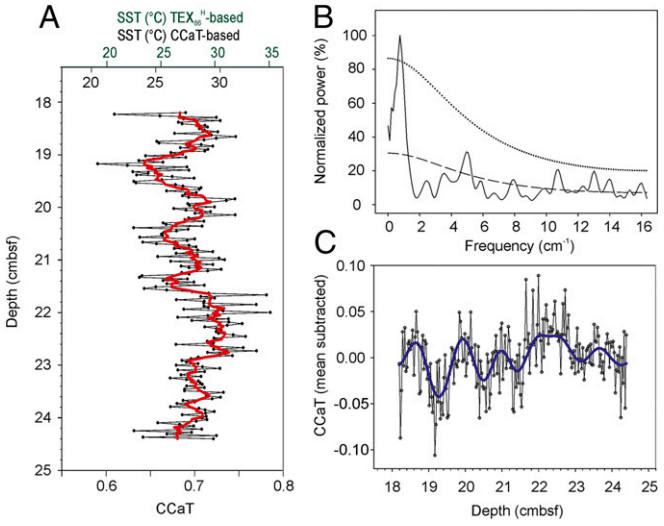

Fig. 3. (*A*) Downcore profile of CCaT and seven-point running average (red line). Data points are average values of ∼15 measurements for each horizon. (*B*) Spectral analysis (REDFIT; 3 segments, Hanning window) for the downcore CCaT values, theoretical red noise (dashed line) and 99% false alarm level (dotted line). (*C*) Mean-subtracted downcore profile of CCaT overlaid with band-pass filtered signals centered at a frequency of 0.79 cycles cm^{-1} (blue line).

Solar Forcing of GDGT Distributions. The CCaT time series was examined for periodic cyclicity by spectral analysis and bandpass filtering of relevant frequencies. Spectral analysis of the CCaT series revealed one single peak with a frequency around 0.75 cycles cm^{-1} that is distinct from red noise and thus is statistically significant (48) (Fig. 3*B*). Subsequent bandpass filtering was optimal when centered at a frequency of 0.79 cycles cm^{-1} (Fig. 3*C*); the compelling match stresses the existence of a major driving force behind CCaT variations. These cyclic variations would not have been observable with conventional high-resolution studies in this setting.

With a sedimentation rate of 6.3 cm ky^{-1} (*Supporting Information*), the observed frequency of 0.75 cycles cm^{-1} corresponds to a cycle length of 212 y. This frequency closely matches the de Vries or Suess cycle of ∼200 y, which, together with the Gleissberg cycle (∼90 y), is among the best-known cycles of solar variation as assessed by the production of cosmogenic radionuclides (^{10}Be, ^{14}C) (49–52). Investigations examining climate forcing by solar variability have been hampered by the need for combining robust proxy records, high resolution, and accurate age assessment. Still, evidence has accumulated over the last decades that confirm the importance of solar forcing in the Holocene (ref. 53 and references therein), and especially an impact on precipitation-evaporation budgets, as evidenced by $\delta^{18}O$ analysis of stalagmites from southern Oman (54, 55) and the Dongge Cave in China (56). Solar influence in the subpolar North Atlantic has been established based on correlations between ^{10}Be and ^{14}C and proxies of drift ice (57) and biological and geochemical data retrieved from lake sediments (58). The vast majority of these studies are land based, but evidence for sun–climate relations is hardly present for the marine realm (53). In the modern Mediterranean Sea, shallow water cores from the Gulf of Taranto served to suggest solar forcing through the observation of significant decadal or centennial cycles in carbonate (59), thermoluminescence (60) or foraminiferal $\delta^{13}C$ (61). A considerable covariance between SST estimated by the alkenone-based $U^{K}_{37'}$ index and atmospheric $\Delta^{14}C$ was also observed from 1,420 to 1,920 (62). Recent modeling efforts (63) identified the potential of the ∼200-y de Vries cycle, but not of the ∼90-y Gleissberg cycle, to impact both surface and middepth water temperature in the Mediterranean Sea.

Long-term amplitude of the alkenone-based SST oscillations described in the modern Gulf of Taranto was 3.4 °C (62), and thus substantially lower than the amplitude suggested by our molecular proxy record that exhibit cyclic amplitudes on the order of 5 °C. As outlined above, signal amplification through a complex, cyclic interplay of archaeal ecology, shifts in seasonality and/or changing water column conditions may have contributed to the high amplitudes of periodic changes of the CCaT. Given robust evidence for a link between Holocene solar cycles and precipitation budgets in Northern Africa (54, 55) and the importance of freshwater supply and especially Nile River runoff for sapropel formation in the eastern Mediterranean (22), cyclic variations in the hydrologic regime on the continent and the

resulting changes in stratification, nutrient input, and redox conditions may have played a major role.

Outlook. This initial study of high-frequency variations of archaeal tetraethers in the sedimentary record demonstrated the enormous potential of this approach to interrogate paleoecological and paleoenvironmental processes at temporal resolutions that were previously inaccessible to the biomarker perspective. The full strength will become apparent in applications to sedimentary settings that enable the construction of records at subannual resolution, and in combination with techniques targeting the inorganic portion of the sediment such as X-ray fluorescence (XRF) scanning (64, 65). The extension of this approach to other informative biomarkers is highly attractive. For example, sedimentary sterols are reflective of the structure of planktonic communities and can be, like the GDGTs, examined via ratios of chemically similar compounds (66) and thus provide information on plankton dynamics. Likewise, long-chain alkenones and the corresponding $U^{K}_{37'}$ index (2) may be amenable to detection by LDI FTICR-MS and further enrich the interpretation of SST records. Comparison of the spatial patchiness of different biomarkers in their sedimentological context could improve our understanding of the ecological and physical mechanisms of molecular proxy formation. Examination of the spatial associations of archaeal core GDGTs and their intact polar precursors could shed light on debated issues regarding the contribution of subseafloor archaea to the archaeal lipid record.

In addition to stratigraphic analysis of the biomarker record in sediments, LDI FTICR-MS may open new avenues for the examination of modern, spatially organized ecosystems, such as redox boundaries in sediments or microbial mats, where lipid biomarker and pigment analysis could reveal ultra-fine community composition. Several of these potentially interesting molecular targets for LDI FTICR-MS will require intense methodological development and possibly demand application of artificial matrix or derivatization techniques [e.g., sterols (67)], but could reward us with a transformative insight into the biomarker world.

Materials and Methods

Sediment Material. The high-resolution analysis was carried out on a sediment section from the gravity core GeoB 15103–1. This core was retrieved by RV *Meteor* in February 2011 during cruise M84-1 (DARCSEAS) from 33°02′N, 32°38′E, in the Levantine Basin, south off Cyprus. Present-day water depth is 1,424 m. The core is archived at the MARUM GeoB core repository (Bremen, Germany).

Steps of Method Validation and Implementation (cf. Fig. S2).

Step 1. To test the capacity of correctly ionizing and identifying GDGTs and to evaluate intrinsic variability of LDI FTICR-MS measurements, the selected test sample known to contain high amounts of GDGTs (see *Supporting Information* for details) was ground, placed on sample holders and analyzed with or without matrix (alpha-cyano-4-hydroxycinnamic acid, HCCA, and dihydroxy benzoic acid, DHB).

Step 2. To evaluate the ability of the LDI method to correctly establish the relative abundance of GDGTs with different numbers of rings (Fig. S1), 21 environmental samples were analyzed with (*i*) the newly developed method and (*ii*) the HPLC/APCI-MS method established in our laboratory for ether lipid analysis, including TEX_{86} determination (19). All samples used for this comparison were obtained during *Meteor* cruise M84-1 [DARCSEAS (46)] and cover a range of burial depths, total organic carbon contents, and sedimentological properties (Table S1).

Step 3. Finally, a high-resolution downcore profile of GDGT distributions was obtained from a 6.2-cm core segment from sapropel 1 at station GeoB15103-1 (46) (Fig. 2*A*). The selected segment with a 5-mm thickness was directly cut out of the core with a custom-made sample pan and dried. Results were later linearly corrected for observed shrinking of the sediment section after drying. After inspection of an undisturbed, even surface, the sample pan was mounted in a standard imaging sample holder (Bruker Daltonics), and a picture was taken before analysis by LDI FTICR-MS. Spatial distribution of GDGTs along this section was achieved by performing a raster with the laser across the sediment section in a regular pattern, with a distance between individual positions of 250 μm. Spot diameter for each position was 175 μm. Assuming a penetration depth of ∼1 μm and a bulk sediment density of ∼1.3 g cm^{-3}, each individual spectrum represents about ∼31 ng of wet sediment; actual penetration depths are expected to depend on sedimentary fabric and might range from ∼1 to 10 μm, with correspondingly differing sample masses.

Instrumental Analysis of GDGTs by LDI FTICR-MS. LDI FTICR-MS analyses were carried out at the Bruker Daltonics facility in Bremen on a 12T solariX FTICR-MS coupled to a DUAL source with Smartbeam II laser (Bruker Daltonics). The FTICR-MS was run in continuous accumulation of selected ions mode (isolation m/z = 1,320; isolation width = 35), to improve the signal-to-noise ratio in the m/z range of isoprenoidal GDGTs (see *Supporting Information* for more details). Although conventional HPLC/APCI-MS analysis separates such compounds chromatographically, LDI FTICR-MS has to completely rely on mass resolution power for proper identification. To differentiate between a GDGT with n cycloalkyl moieties and the second isotopic peak of a GDGT with one more moiety, resolution has to exceed 150,000 at the m/z ratio of 1,300. We cannot rule out that sedimentary intact polar GDGTs contribute to the recorded signal due to their potential degradation during laser-based desorption, but this influence is probably small due to the protective effect of sediment matrix and the typically relatively low proportion of intact relative to total GDGTs (68). Automatic spatially resolved measurements were carried out using FlexImaging 4.0 and FTMSControl 2.0 (Bruker Daltonics). The spectra acquired from each position contain m/z and intensity information representative of the compounds at that position. For details on data processing see *Supporting Information*.

Instrumental Analysis of GDGTs by HPLC/APCI-MS. Samples were extracted following a modified Bligh and Dyer method (69). HPLC/APCI-MS analysis of GDGTs was carried out following the method developed by (19) (see *Supporting Information* for more details).

X-Ray Fluorescence Analysis. The vertical extension of sapropel 1 in the sediment core at location GeoB 15103 was confirmed by XRF scanning to refine our estimate of sedimentation rates and thus establish a temporal framework for the relationship with solar cycles (see *Supporting Information* for more details).

ACKNOWLEDGMENTS. We are grateful to the participating scientists and ship crews of cruise M84/1 (DARCSEAS) and to Kevin Becker for the characterization of samples from this cruise. Special thanks to Dr. John M. Hayes and Dr. Boris Koch for their helpful comments on an earlier version of this manuscript, and to Dr. Michael Schulz for his support in performing spectral analysis. The study was funded by the European Research Council under the European Union's (EU) Seventh Framework Programme, "Ideas" Specific Programme, ERC Grant Agreement 247153 [Advanced Grant DARCLIFE (to K.-U.H.)] and by the Deutsche Forschungsgemeinschaft (DFG) through Grants Inst 144/300-1 (LC-QTOF system), HI616/10-1 (to K.-U.H.), LI1901/1-1 (to J.S.L.), and the DFG-Research Center and Excellence Cluster 'The Ocean in the Earth System.' P.L.B.'s work on the application of multivariate analyses to microbial ecology datasets is supported by the EU's FP7 (Joint Call OCEAN.2011–2: Marine microbial diversity—new insights into marine ecosystems functioning and its biotechnological potential), Grant Agreement 287589 (MicroB3).

1. Didyk BM, Simoneit BRT, Brassell SC, Eglinton G (1978) Organic geochemical indicators of paleo-environmental conditions of sedimentation. *Nature* 272(5650):216–222.
2. Brassell SC, Eglinton G, Marlowe IT, Pflaumann U, Sarnthein M (1986) Molecular stratigraphy - A new tool for climatic assessment. *Nature* 320(6058):129–133.
3. Schouten S, Hopmans EC, Schefuss E, Damste JSS (2002) Distributional variations in marine crenarchaeotal membrane lipids: A new tool for reconstructing ancient sea water temperatures? *Earth Planet Sci Lett* 204(1-2):265–274.
4. Hinrichs KU, Hmelo LR, Sylva SP (2003) Molecular fossil record of elevated methane levels in late Pleistocene coastal waters. *Science* 299(5610):1214–1217.
5. Pearson A, Ingalls AE (2013) Assessing the use of archaeal lipids as marine environmental proxies. *Annu Rev Earth Planet Sci* 41:359–384.
6. Reed WE, Mankiewicz P (1975) Molecular stratigraphy. *Nature* 254(5496):127–129.
7. Kennedy JA, Brassell SC (1992) Molecular records of 20th-century El Niño events in laminated sediments from the Santa Barbara basin. *Nature* 357(6373):62–64.
8. Huguet C, et al. (2007) A study of the TEX_{86} paleothermometer in the water column and sediments of the Santa Barbara Basin, California. *Paleoceanography* 22(3):PA3203.
9. Kuypers MMM, et al. (2001) Massive expansion of marine archaea during a mid-Cretaceous oceanic anoxic event. *Science* 293(5527):92–95.

10. Schouten S, et al. (2003) Extremely high sea-surface temperatures at low latitudes during the middle Cretaceous as revealed by archaeal membrane lipids. *Geology* 31(12):1069–1072.
11. Oger PM, Cario A (2013) Adaptation of the membrane in Archaea. *Biophys Chem* 183: 42–56.
12. Shimada H, Nemoto N, Shida Y, Oshima T, Yamagishi A (2008) Effects of pH and temperature on the composition of polar lipids in *Thermoplasma acidophilum* HO-62. *J Bacteriol* 190(15):5404–5411.
13. Boyd ES, et al. (2011) Temperature and pH controls on glycerol dibiphytanyl glycerol tetraether lipid composition in the hyperthermophilic crenarchaeon *Acidilobus sulfurireducens*. *Extremophiles* 15(1):59–65.
14. Gliozzi A, Paoli G, De Rosa M, Gambacorta A (1983) Effect of isoprenoid cyclization on the transition-temperature of lipids in thermophilic archaebacteria. *Biochim Biophys Acta* 735(2):234–242.
15. Jenkyns HC, Forster A, Schouten S, Sinninghe Damsté JS (2004) High temperatures in the Late Cretaceous Arctic Ocean. *Nature* 432(7019):888–892.
16. Castañeda IS, et al. (2010) Millennial-scale sea surface temperature changes in the eastern Mediterranean (Nile River Delta region) over the last 27,000 years. *Paleoceanography* 25(1):PA1208.
17. Schouten S, Hopmans EC, Damste JSS (2013) The organic geochemistry of glycerol dialkyl glycerol tetraether lipids: A review. *Org Geochem* 54:19–61.
18. Hopmans EC, Schouten S, Pancost RD, van der Meer MTJ, Sinninghe Damsté JS (2000) Analysis of intact tetraether lipids in archaeal cell material and sediments by high performance liquid chromatography/atmospheric pressure chemical ionization mass spectrometry. *Rapid Commun Mass Spectrom* 14(7):585–589.
19. Becker KW, Lipp JS, Zhu C, Liu X-L, Hinrichs K-U (2013) An improved method for the analysis of archaeal and bacterial ether core lipids. *Org Geochem* 61:34–44.
20. Knochenmuss R (2006) Ion formation mechanisms in UV-MALDI. *Analyst (Lond)* 131(9):966–986.
21. Fuchs B, Süss R, Schiller J (2010) An update of MALDI-TOF mass spectrometry in lipid research. *Prog Lipid Res* 49(4):450–475.
22. Rossignol-Strick M, Nesteroff W, Olive P, Vergnaudgrazzini C (1982) After the deluge - Mediterranean stagnation and sapropel formation. *Nature* 295(5845):105–110.
23. Sachs JP, Repeta DJ (1999) Oligotrophy and nitrogen fixation during eastern Mediterranean sapropel events. *Science* 286(5449):2485–2488.
24. de la Torre JR, Walker CB, Ingalls AE, Könneke M, Stahl DA (2008) Cultivation of a thermophilic ammonia oxidizing archaeon synthesizing crenarchaeol. *Environ Microbiol* 10(3):810–818.
25. Pitcher A, et al. (2010) Crenarchaeol dominates the membrane lipids of Candidatus Nitrososphaera gargensis, a thermophilic group I.1b Archaeon. *ISME J* 4(4):542–552.
26. Zhang YG, et al. (2011) Methane index: A tetraether archaeal lipid biomarker indicator for detecting the instability of marine gas hydrates. *Earth Planet Sci Lett* 307(3-4):525–534.
27. Liu X-L, Lipp JS, Schroeder JM, Summons RE, Hinrichs K-U (2012) Isoprenoid glycerol dialkanol diethers: A series of novel archaeal lipids in marine sediments. *Org Geochem* 43:50–55.
28. Kim J-H, et al. (2010) New indices and calibrations derived from the distribution of crenarchaeal isoprenoid tetraether lipids: Implications for past sea surface temperature reconstructions. *Geochim Cosmochim Acta* 74(16):4639–4654.
29. Ho SL, et al. (2014) Appraisal of TEX_{86} and TEX_{86}^{L} thermometries in subpolar and polar regions. *Geochim Cosmochim Acta* 131:213–226.
30. Borcard D, Legendre P (2002) All-scale spatial analysis of ecological data by means of principal coordinates of neighbour matrices. *Ecol Modell* 153(1-2):51–68.
31. Borcard D, Legendre P, Avois-Jacquet C, Tuomisto H (2004) Dissecting the spatial structure of ecological data at multiple scales. *Ecology* 85(7):1826–1832.
32. Dray S, Legendre P, Peres-Neto PR (2006) Spatial modelling: A comprehensive framework for principal coordinate analysis of neighbour matrices (PCNM). *Ecol Modell* 196(3-4):483–493.
33. Locarnini RA, et al. (2013) World Ocean Atlas 2013, Volume 1: Temperature. *NOAA Atlas NESDIS 73*, eds Levitus S & Mishonov A (National Oceanographic Data Center, Silver Spring, MD).
34. Rossignol-Strick M (1999) The Holocene climatic optimum and pollen records of sapropel 1 in the eastern Mediterranean, 9000-6000 BP. *Quat Sci Rev* 18(4-5):515–530.
35. Galand PE, Gutierrez-Provecho C, Massana R, Gasol JM, Casamayor EO (2010) Inter-annual recurrence of archaeal assemblages in the coastal NW Mediterranean Sea (Blanes Bay Microbial Observatory). *Limnol Oceanogr* 55(5):2117–2125.
36. Herfort L, et al. (2007) Variations in spatial and temporal distribution of Archaea in the North Sea in relation to environmental variables. *FEMS Microbiol Ecol* 62(3):242–257.
37. Francis CA, Roberts KJ, Beman JM, Santoro AE, Oakley BB (2005) Ubiquity and diversity of ammonia-oxidizing archaea in water columns and sediments of the ocean. *Proc Natl Acad Sci USA* 102(41):14683–14688.
38. Church MJ, Wai B, Karl DM, DeLong EF (2010) Abundances of crenarchaeal amoA genes and transcripts in the Pacific Ocean. *Environ Microbiol* 12(3):679–688.
39. Karner MB, DeLong EF, Karl DM (2001) Archaeal dominance in the mesopelagic zone of the Pacific Ocean. *Nature* 409(6819):507–510.
40. Hernandez-Sanchez MT, Woodward EMS, Taylor KWR, Henderson GM, Pancost RD (2014) Variations in GDGT distributions through the water column in the South East Atlantic Ocean. *Geochim Cosmochim Acta* 132:337–348.
41. Koutavas A, Demenocal PB, Olive GC, Lynch-Stieglitz J (2006) Mid-Holocene El Nino-Southern Oscillation (ENSO) attenuation revealed by individual foraminifera in eastern tropical Pacific sediments. *Geology* 34(12):993–996.
42. Leduc G, Vidal L, Cartapanis O, Bard E (2009) Modes of eastern equatorial Pacific thermocline variability: Implications for ENSO dynamics over the last glacial period. *Paleoceanography* 24(3):PA3202.
43. Leider A, Hinrichs K-U, Mollenhauer G, Versteegh GJM (2010) Core-top calibration of the lipid-based U^{K}_{37}' and TEX_{86} temperature proxies on the southern Italian shelf (SW Adriatic Sea, Gulf of Taranto). *Earth Planet Sci Lett* 300(1-2):112–124.
44. Wakeham SG, et al. (2012) Biomarkers, chemistry and microbiology show chemoautotrophy in a multilayer chemocline in the Cariaco Basin. *Deep Sea Res Part I Oceanogr Res Pap* 63:133–156.
45. Emeis K-C, et al. (1996) *Proceedings of the Ocean Drilling Program, Initial Reports* 160 (Ocean Drilling Program, College Station, TX).
46. Zabel M (2012) RV METEOR, Cruise Report M84/L1. Biogeochemistry and methane hydrates of the Black Sea; Oceanography of the Mediterranean; Shelf sedimentation and cold water carbonates 2012 (DFG Senatskommission für Ozeanographie, Bremen, Germany).
47. Wakeham SG, Lewis CM, Hopmans EC, Schouten S, Damste JSS (2003) Archaea mediate anaerobic oxidation of methane in deep euxinic waters of the Black Sea. *Geochim Cosmochim Acta* 67(7):1359–1374.
48. Schulz M, Mudelsee M (2002) REDFIT: Estimating red-noise spectra directly from unevenly spaced paleoclimatic time series. *Comput Geosci* 28(3):421–426.
49. Stuiver M, Braziunas TF (1993) Sun, ocean, climate and atmospheric $^{14}CO_2$: An evaluation of causal and spectral relationships. *Holocene* 3:289–305.
50. Wagner G, et al. (2001) Presence of the solar de Vries cycle (similar to 205 years) during the last ice age. *Geophys Res Lett* 28(2):303–306.
51. Peristykh AN, Damon PE (2003) Persistence of the Gleissberg 88-year solar cycle over the last similar to 12,000 years: Evidence from cosmogenic isotopes. *J Geophys Res-Space Phys* 108(A1).
52. Knudsen MF, et al. (2009) Taking the pulse of the Sun during the Holocene by joint analysis of ^{14}C and ^{10}Be. *Geophys Res Lett* 36(16):L16701.
53. Versteegh GJM (2005) Solar forcing of climate. 2: Evidence from the past. *Space Sci Rev* 120(3-4):243–286.
54. Fleitmann D, et al. (2003) Holocene forcing of the Indian monsoon recorded in a stalagmite from southern Oman. *Science* 300(5626):1737–1739.
55. Neff U, et al. (2001) Strong coherence between solar variability and the monsoon in Oman between 9 and 6 kyr ago. *Nature* 411(6835):290–293.
56. Wang Y, et al. (2005) The Holocene Asian monsoon: Links to solar changes and North Atlantic climate. *Science* 308(5723):854–857.
57. Bond G, et al. (2001) Persistent solar influence on North Atlantic climate during the Holocene. *Science* 294(5549):2130–2136.
58. Hu FS, et al. (2003) Cyclic variation and solar forcing of Holocene climate in the Alaskan subarctic. *Science* 301(5641):1890–1893.
59. Cini Castagnoli G, Bonino G, Provenzale A, Serio M, Callegari E (1992) The $CaCO_3$ profiles of deep and shallow Mediterranean-Sea cores as indicators of past solar-terrestrial relationships. *Nuovo Cimento C* 15(5):547–563.
60. Cini Castagnoli G, Bonino G, DellaMonica P, Taricco C (1997) Record of thermoluminescence in sea sediments in the last millennia. *Nuovo Cimento C* 20(1):1–8.
61. Cini Castagnoli G, Taricco C, Alessio S (2005) Isotopic record in a marine shallow-water core: Imprint of solar centennial cycles in the past 2 millennia. *Adv Space Res-Series* 35(3):504–508.
62. Versteegh GJM, de Leeuw JW, Taricco C, Romero A (2007) Temperature and productivity influences on UK37′ and their possible relation to solar forcing of the Mediterranean winter. *Geochem Geophy Geosy* 8.
63. Seidenglanz A, Prange M, Varma V, Schulz M (2012) Ocean temperature response to idealized Gleissberg and de Vries solar cycles in a comprehensive climate model. *Geophys Res Lett* 39(22):L22602.
64. Röhl U, Abrams LJ (2000) 11. High resolution, downhole, and nondestructive core measurements from sites 999 and 1001 in the Caribbean Sea: Application to the late Paleocene thermal maximum. *Proceedings of the Ocean Drilling Program, Scientific Results*, eds Leckie RM, Sigurdsson H, Acton GD, & Draper G (Ocean Drilling Program, College Station, TX).
65. Richter TO, et al. (2006) The Avaatech XRF Core Scanner: Technical description and applications to NE Atlantic sediments. *Geol Soc Lond Spec Publ* 267(1):39–50.
66. Huang WY, Meinschein WG (1979) Sterols as ecological indicators. *Geochim Cosmochim Acta* 43(5):739–745.
67. Hailat I, Helleur RJ (2014) Direct analysis of sterols by derivatization matrix-assisted laser desorption/ionization time-of-flight mass spectrometry and tandem mass spectrometry. *Rapid Commun Mass Spectrom* 28(2):149–158.
68. Liu X, Lipp JS, Hinrichs K-U (2011) Distribution of intact and core GDGTs in marine sediments. *Org Geochem* 42(4):368–375.
69. Sturt HF, Summons RE, Smith K, Elvert M, Hinrichs KU (2004) Intact polar membrane lipids in prokaryotes and sediments deciphered by high-performance liquid chromatography/electrospray ionization multistage mass spectrometry—New biomarkers for biogeochemistry and microbial ecology. *Rapid Commun Mass Spectrom* 18(6):617–628.